


Enzyme-Enriched Condensates Show Self-Propulsion, Positioning, and Coexistence

Leonardo Demarchi^{1,*}, Andriy Goychuk^{1,†,‡}, Ivan Maryshev¹, and Erwin Frey^{1,2,§}¹Arnold Sommerfeld Center for Theoretical Physics and Center for NanoScience, Department of Physics, Ludwig-Maximilians-Universität München, Theresienstraße 37, D-80333 München, Germany²Max Planck School Matter to Life, Hofgartenstraße 8, D-80539 München, Germany (Received 29 September 2022; accepted 3 February 2023; published 20 March 2023)

Enzyme-enriched condensates can organize the spatial distribution of their substrates by catalyzing nonequilibrium reactions. Conversely, an inhomogeneous substrate distribution induces enzyme fluxes through substrate-enzyme interactions. We find that condensates move toward the center of a confining domain when this feedback is weak. Above a feedback threshold, they exhibit self-propulsion, leading to oscillatory dynamics. Moreover, catalysis-driven enzyme fluxes can lead to interrupted coarsening, resulting in equidistant condensate positioning, and to condensate division.

DOI: 10.1103/PhysRevLett.130.128401

Liquid-liquid phase separation in living cells can lead to the formation of biomolecular condensates that aid intracellular organization [1–7]. These condensates have different functions such as compartmentalization of reactions [4], buffering of molecules [8], and midcell localization during cell division [9]. However, in a thermal equilibrium system, the liquids will completely segregate through a coarsening process (Ostwald ripening) [10–13]. To arrest this process, the system must be brought out of equilibrium by supplying energy, e.g., via fuel-driven chemical reactions. This has been shown to lead to “active droplet” systems that exhibit a wealth of novel phenomena not encountered in thermal equilibrium [3,6,14].

Previous studies have considered systems with a continuous turnover of condensate (droplet) material by chemical reactions [14–24]. The resulting material fluxes lead to multidroplet coexistence [18,19,22–24] and droplet division [21]. Here, we study a different class of systems where conserved enzymes spontaneously phase separate, or localize to an existing condensate [25]. These enzymes then regulate reactions among other molecules by transiently binding substrate and catalyzing its conversion into product via a lower activation barrier. For example, in the bacterium *Myxococcus xanthus*, a PomXY cluster (moving on the nucleoid) regulates the cycling of PomZ between two conformations [9,31–33]. We show that such substrate turnover and the resulting enzyme fluxes lead to condensate self-propulsion, positioning, interrupted coarsening, and condensate division. Interestingly, previous studies have

shown that liquid droplets can self-propel on a surface through active stresses [34–39], altering their wetting properties [40,41], or in viscous fluids through Marangoni flows [42]. In contrast, in our case, condensate motion is driven by the bulk interactions between the various chemical species and does not require surfaces or hydrodynamic coupling.

While condensates might consist of several components, here we focus on the enzyme concentration $c(\mathbf{x}, t)$. To describe the dynamics of liquid-liquid phase separation, we take the Cahn-Hilliard equation as a starting point with the following chemical potential [43]: $\mu_0(c) = -r(c - \tilde{c}) + u(c - \tilde{c})^3 - \kappa \nabla^2 c$. This chemical potential $\mu_0(c) = \delta \mathcal{F}[c]/\delta c$ corresponds to the Ginzburg-Landau free energy functional $\mathcal{F}[c]$ for a symmetric binary mixture with the critical density \tilde{c} and phenomenological parameters r , u , and κ ; in particular, the control parameter r measures the distance from the critical point [13]. The enzymes interact with substrates and products, which are present at concentrations $s(\mathbf{x}, t)$ and $p(\mathbf{x}, t)$. These couplings, quantified by the Flory-Huggins (FH) parameters χ_s and χ_p , modify the local chemical potential of enzymes. Assuming that the particle currents are proportional to gradients in the chemical potential [44,45], the enzyme dynamics is given by

$$\partial_t c(\mathbf{x}, t) = \nabla \cdot [M c \nabla (\mu_0(c) + \chi_s s + \chi_p p)], \quad (1)$$

where M denotes a mobility and the term in the square brackets is the enzyme flux $\mathbf{j}(\mathbf{x}, t)$. This “gradient dynamics” leads to a gradual minimization of the free energy functional from which it is derived [25], a hallmark of systems close to thermal equilibrium. Analogously, the thermodynamic fluxes of substrates and products can be derived from the same free energy functional [25].

Active systems, however, exhibit processes that break detailed balance in protein reaction networks [46,47].

Published by the American Physical Society under the terms of the Creative Commons Attribution 4.0 International license. Further distribution of this work must maintain attribution to the author(s) and the published article's title, journal citation, and DOI.

For example, in the conversion of nucleoside triphosphatases (NTPases) between an NDP-bound (“product”) and a less stable NTP-bound (“substrate”) state, abundance of NTP (nucleoside triphosphate, “fuel”) in solution may shift the equilibrium toward the latter [48] and replenish substrate with the net rate k_2p . Transient binding of an enzyme (NTPase-activating protein) to substrate can, by lowering the activation barrier of hydrolysis, kinetically select the fuel-independent reaction pathway and replenish product with the net rate k_1cs , which follows from the law of mass action. We assume that these separate reaction pathways are far from their respective equilibria, so that we can disregard thermodynamic constraints [44,49] and treat the rate constants $k_{1,2}$ as independent parameters [25]. Hence, we write for the dynamics of the substrate and the product:

$$\partial_t s = \nabla \cdot (D \nabla s + \Lambda s \chi_s \nabla c) - k_1 cs + k_2 p, \quad (2a)$$

$$\partial_t p = \nabla \cdot (D \nabla p + \Lambda p \chi_p \nabla c) + k_1 cs - k_2 p. \quad (2b)$$

Catalytic substrate turnover is preceded by enzyme binding, suggesting effective pairwise attraction, $\chi_s < 0$. Converting substrate into product reduces its affinity for the enzymes, $\chi_s < \chi_p$, leading to unbinding. Note that in Eq. (2) we have taken the liberty of formally decoupling the diffusion coefficient D from the mobility Λ , thus introducing a further source of far from equilibrium dynamics by breaking the fluctuation-dissipation relation valid for thermal equilibrium systems. In the present context, this is the Einstein-Smoluchowsky relation $D = \Lambda k_B T$ [50]. With the aim of simplifying the analysis, in the present work we consider $\Lambda = 0$, an approximation that is valid for weak FH parameters $\chi_{s,p}$ and will be addressed elsewhere [51].

For our initial exploration of the dynamics, we consider a finite-sized domain $[-L, L]$ in a one-dimensional (1D) geometry with no-flux boundary conditions at $x = \pm L$. A droplet then corresponds to a plateau with a high enzyme concentration, surrounded by an enzyme-poor phase (Fig. 1). If the width of the interface between these phases, $w = \sqrt{2\kappa/r}$, is much smaller than all other length scales, one can use a sharp interface approximation with piecewise constant concentration c . For our analysis, we consider weak interactions, $|\chi_s s| + |\chi_p p| \ll r(c_+ - c_-)$, and therefore approximate the enzyme concentrations in the two phases by their equilibrium values, $c_{\pm} = \tilde{c} \pm \sqrt{r/u}$.

First, consider a *stationary* droplet, where a closed analytic solution of Eqs. (1) and (2) can be obtained [25]. The stationary state is maintained by a balance of reactive and diffusive fluxes (Fig. 1). In the droplet, the enzymes catalyze the conversion of substrate to product, consuming the former and accumulating the latter. Diffusive fluxes in turn replenish substrate in the droplet while expelling product, resulting in concentration gradients over the characteristic diffusion lengths $l_{\pm} = \sqrt{D/(k_1 c_{\pm} + k_2)}$

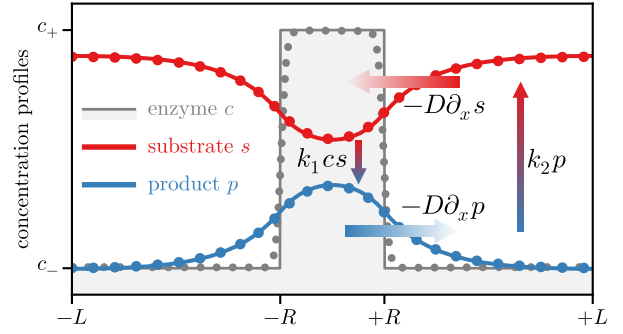


FIG. 1. Steady-state concentration profiles for a 1D droplet with no-flux boundary conditions at $x = \pm L$. Arrows indicate reactive (vertical) and diffusive (horizontal) fluxes. The analytical solutions in the sharp interface approximation (lines) match our simulations (dots). We use c_+ as reference concentration and define the characteristic time $\tau_0 := k_2^{-1}$, diffusion length in the absence of enzymes $l_0 := \sqrt{D/k_2}$, and reference energy $\epsilon_0 := rc_+$. The remaining parameters, $c_- = 0.1c_+$, $w = 0.1l_0$, $R = l_0$, $L = 5l_0$, $M = 100D/\epsilon_0$, $k_1 = k_2/c_+$, $\chi_s = -0.05r$, $\chi_p = -0.01r$, and $s + p = c_+$, are fixed for all figures unless stated otherwise.

inside and outside the droplet, respectively. This leads to cyclic diffusive and reactive fluxes such that time-reversal symmetry is broken and one has a reaction-driven non-equilibrium steady state.

If there is an appreciable difference in substrate or product concentration between the two droplet interfaces (henceforth referred to as “imbalance”), this generally results in a chemical potential gradient that can drive droplet motion through a net flux of enzymes [Eq. (1)]. Indeed, using finite element (FEM) simulations of Eqs. (1) and (2), we find a broad parameter regime with ballistic droplet motion [Fig. 2(c), Video 1]. To analytically determine the conditions for the onset of this *self-propulsion instability*, we next study the sharp-interface limit of a single 1D droplet in an infinite domain.

Similar to the analysis of Fisher waves [52], we solve Eq. (2) in the reference frame of a moving droplet to obtain the concentration profiles of substrates and products, and then use Eq. (1) to derive a self-consistency relation for the droplet velocity v . Specifically, the continuity equation, Eq. (1), implies that the moving steady-state enzyme profile, $c(z)$ with $z := x - vt$ and constant velocity v , can only be maintained if $\partial_z j(z) = v \partial_z c(z)$ holds at all times. The local flux of enzymes is therefore given by $j(z) = v[c(z) - c_-]$, and vanishes in the far field where all concentrations become homogeneous [25]. The concentration of enzymes in the droplet is enriched by $\Delta c = c_+ - c_-$ with respect to the far-field value $c(\pm\infty) = c_-$. While the enzyme flux is driven by the *local* chemical potential and concentration gradients [Eq. (1)], integrating the flux over the droplet domain $[-R, R]$ yields an expression that depends only on the values at the droplet boundaries. In the sharp-interface limit, the μ_0 term

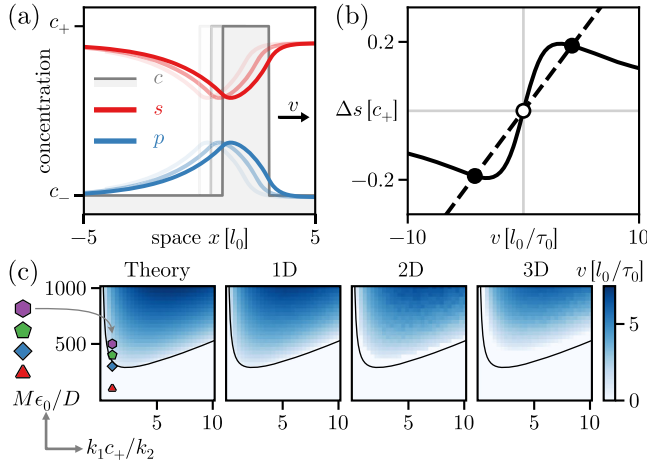


FIG. 2. Self-propulsion instability. (a) Analytical profiles for a droplet moving with velocity $v = 2l_0/\tau_0$. Lighter colors indicate earlier times. (b) Graphical analysis of the self-consistency relation, Eq. (3), for $M\epsilon_0/D = 1000$. The solid curve indicates the substrate imbalance $\Delta s(v)$, while the slope of the dashed line corresponds to the right-hand side of inequality, Eq. (4). Stationary droplets correspond to unstable solutions (empty circle), while self-propelling droplets are stable (filled circles). (c) Theoretical prediction and simulation results for the self-propulsion velocity (color scale) with M and k_1 as free parameters. The solid black lines indicate the critical mobility M^* (for the explicit closed expression see [25]).

becomes mirror-symmetric relative to the droplet center and hence does not contribute to the self-consistency relation for the droplet velocity:

$$2R\Delta c v = -M c_+ [\chi_s \Delta s(v) + \chi_p \Delta p(v)]. \quad (3)$$

Here, $\Delta s(v) = s(R) - s(-R)$ is the substrate concentration imbalance between the two opposite sides of the droplet, with an analogous expression $\Delta p(v)$ for the product. This result quantifies how asymmetric substrate and product concentration profiles drive droplet motion.

Using the closed analytic expressions for the substrate concentration profiles [25], shown in Fig. 2(a), one can graphically solve the self-consistency relation, Eq. (3), for the droplet velocity v [Fig. 2(b)]. Specifically, for $\Lambda = 0$, where the total concentration of substrates and products is constant [Eq. (2)], the right-hand side of Eq. (3) simplifies to $M c_+ (\chi_p - \chi_s) \Delta s(v)$. Based on the graphical form of $\Delta s(v)$, a nonvanishing solution to the self-consistency relation for the velocity v exists if [Fig. 2(b)]:

$$\frac{\partial}{\partial v} \Delta s(v)|_{v=0} > \frac{2R\Delta c}{M c_+ (\chi_p - \chi_s)}. \quad (4)$$

Thus, traveling wave solutions emerge if, for example, the mobility M or the difference between the FH parameters $\chi_p - \chi_s$ are sufficiently large. Then, enzymes are pulled

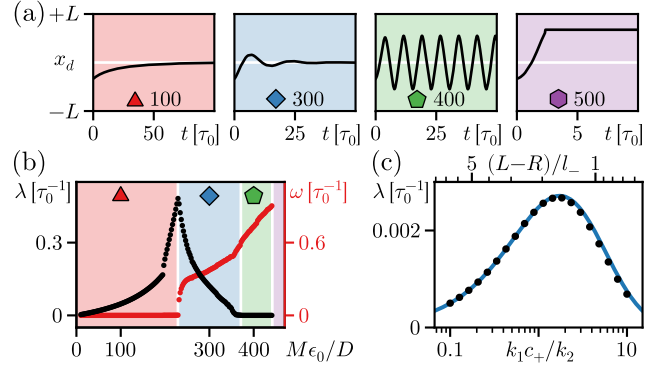


FIG. 3. Self-centering and oscillations. (a) Droplet center trajectories in simulations for different values of M ; symbols indicate the position in the diagram shown in Fig. 2(c). The droplet center is initially at $x_d(0) = -l_0$ in a domain of size $L = 3l_0$. (b) Decay rate (black dots) and frequency (red dots) as functions of M , obtained by fitting the respective droplet trajectories. Red triangle indicates overdamped regime. (c) Relaxation rate λ as a function of k_1 (bottom axis), for $M\epsilon_0/D = 10$ and $x_d(0) = -0.3l_0$. Top axis relates the domain size to the length scale of the concentration profiles. The analytical predictions (blue line) in the quasi-steady-state approximation [25] match our simulations (black dots).

more toward substrates than products, so that enzymatic substrate depletion can induce a chemophoretic effect. This theoretical analysis quantitatively explains the onset of the self-propulsion instability that we observed in our simulations; see Fig. 2(c) for a comparison.

Droplet movement is driven by asymmetries in the concentration profiles of substrates and products. Droplets induce such asymmetries autonomously during self-propulsion but also near impermeable domain boundaries. Figure 3(a) and Video 2 show the results of FEM simulations in a closed domain for four characteristic values of the mobility M . Below the self-propulsion threshold M^* , the droplet exhibits an overdamped relaxation toward the domain center (red), where the concentration profiles become symmetric. Thus, the impermeable domain boundaries effectively repel the droplet, due to substrate depletion and product enrichment within a range l_- . When increasing M^* , there is a transition from overdamped to underdamped oscillatory relaxation (blue), where the relaxation rate λ has a maximum at critical damping [Fig. 3(b)], similar to a damped harmonic oscillator. Above the self-propulsion threshold M^* , droplets autonomously accelerate to a terminal velocity v [Fig. 2(c)]. Instead of droplet self-centering, one then observes oscillations (green) with frequency $\omega \approx v/(L - l_-)$, where the domain boundaries cause droplets to slow down and reverse. Droplets with strong self-propulsion (purple) can overcome this repulsion and attach to the boundary.

To elucidate how droplet self-centering depends on the reaction rates, we analyzed the overdamped regime, in

which droplet motion is much slower than the relaxation of the substrate and product concentration profiles. This timescale separation allows one to solve Eq. (2) analytically using a quasistationary approximation, where the substrate and product concentration profiles are in steady state with the droplet center $x_d(t)$ considered as slowly varying. The obtained steady-state profiles are asymmetric when the droplet is not centered in the domain, if and only if the characteristic length l_+ is neither much larger nor much smaller than the droplet size R (lest both droplet interfaces have equal concentrations). These asymmetric concentration profiles induce droplet motion toward the domain center, see Eq. (3), with a velocity $v(x_d)$ that we linearize as a function of the distance to the domain center [25], $|x_d| \ll l_-$. The resulting approximation for the relaxation rate λ agrees well with our simulations [Fig. 3(c)], and demonstrates that droplet self-centering is fastest for a finite value of $k_1 c_+ / k_2$. Moreover, our analysis and simulations show that droplet self-centering proceeds fastest when the distance between the droplet interface and the domain boundary is comparable to the range of repulsion, $L - R \sim l_-$ [Fig. 3(c)].

A state with multiple droplets cannot be stable in a thermodynamic system. Instead, a coarsening process driven by interfacial energy minimization takes place, causing smaller droplets to shrink and larger droplets to grow until there is complete phase separation [11–13]. As our system is out of equilibrium, it can result in a stable coexistence of multiple droplets. Specifically for the system we are considering, larger droplets have a larger enzymatic activity and hence consume more substrate, leading to a reduced substrate concentration at their interfaces. This results in a gradient of substrate (and product) in the low-concentration phase between droplets of different sizes, thereby transporting enzymes from the larger to the smaller droplets and thus counteracting the coarsening process [Eq. (1)].

For a 1D system, the thermodynamic coarsening process described by the Cahn-Hilliard model is extraordinarily slow with the average droplet radius growing only logarithmically with time [13]. Hence, one expects that (even weak) enzymatic processes can interrupt coarsening. Indeed, solving the dynamics of multiple droplets analytically in the adiabatic limit [25], we find enzyme fluxes between pairs of differently sized droplets, which are proportional to the difference in the substrate concentration at their closest interfaces. These currents stop the coarsening process and lead to a steady state where the droplets position themselves equidistantly to each other to even out concentration imbalances between all interfaces (Video 4).

For 2D and 3D systems, Ostwald ripening is dominated by surface tension effects (Laplace pressure) and the ensuing law for droplet growth becomes a power law [13]. In this case, one intuitively expects that the coarsening process can be interrupted only if the mass fluxes of the

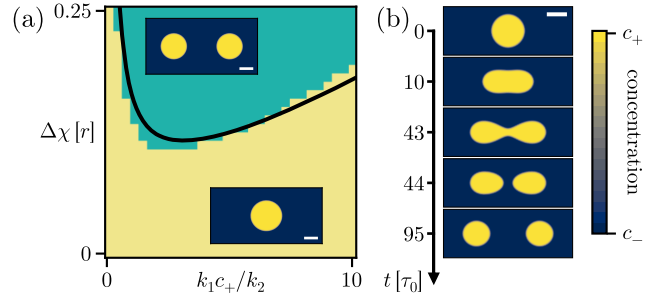


FIG. 4. Coexistence and division of 3D droplets. We consider $Mc_0/D = 10$ and $w = 0.05l_0$. Scale bars indicate unit length $l_0 := \sqrt{D/k_2}$. (a) Simulated pairs of droplets with different initial radii $R_1 = 1.1l_0$ and $R_2 = 0.9l_0$ either stay separated (cyan regime) or coalesce (yellow regime) depending on k_1 and on the difference in FH parameters $\Delta\chi = \chi_p - \chi_s$. Solid black line corresponds to analytical estimate, Eq. (5), for $\Delta\chi^*(k_1)$. (b) Simulation snapshots demonstrating a droplet division in 3D. We observed droplet divisions only for very strong attraction of enzymes toward substrates, here $\chi_s/r = -0.5$.

enzymes are sufficiently strongly coupled to the concentration of the products and substrates [53,54]. Figure 4(a) shows FEM simulation results for a 3D system with a pair of droplets, which confirm this intuitive argument. The existence of a coarsening threshold for 3D systems can also be understood analytically as a balance between a coarsening current due to surface tension and a mass flux of enzymes driven by reaction-maintained product and substrate concentration gradients. We estimate the former using the standard Gibbs-Thomson relation [13,14] and the latter by adapting the above results for the 1D system [25]. By comparing the two currents we find the following estimate for the critical difference between the FH parameters $\Delta\chi = \chi_p - \chi_s$ above which one expects droplet coexistence, i.e., interrupted coarsening:

$$\Delta\chi^* = \frac{2}{3} \frac{rw\Delta c/\Delta s^* [l_+^{-1} \cosh(\xi) + l_-^{-1} \sinh(\xi)]^2}{l_+^{-1} [\sinh(2\xi) - 2\xi] + 2l_-^{-1} [\sinh^2(\xi) - \xi^2]}, \quad (5)$$

where $\xi := \bar{R}/l_+$ is the ratio of the average droplet radius to the typical length scale of the concentration gradients inside of a droplet, and Δs^* is the difference between the local equilibria of substrate in the two phases [25]. Notwithstanding the partially heuristic nature of the derivation, our estimate yields a good approximation for the boundary between coexistence and coarsening in parameter space [Fig. 4(a)].

In our numerical simulations, we also observed that initially spherical droplets can undergo a shape instability and elongate in one direction for large enough values of $\Delta\chi$ [25]. Once sufficiently elongated, 3D droplets form a neck and divide (Fig. 4, Video 5), which we speculate to occur

through a pearling instability driven by surface tension [55] independent of the preceding shape instability. This droplet division process is driven by intermolecular interactions that induce conservative enzyme fluxes, as opposed to Ref. [21] where the droplet material is cyclically produced and degraded, leading to nonconservative fluxes and droplet growth.

We have analyzed the nonequilibrium dynamics of enzyme-enriched condensates, whose enzymatic activity guides the generation of inhomogeneous substrate and product concentration profiles that, in turn, drive condensate motion. Conceptually, this corresponds to a feedback mechanism in which, for example, an NTPase such as PomZ undergoing a cycle of hydrolysis ($s \rightarrow p$, catalyzed by a NTPase-activating protein c) and nucleotide exchange ($p \rightarrow s$) generates concentration gradients of its two different chemical states (s and p) that drive droplet movement through a process akin to chemophoresis. Our results show that such a generic mechanism results in equidistant positioning of condensates in closed domains, persistent condensate motion, and even shape instabilities that lead to condensate division. We speculate that this mechanism, in its basic form, may be relevant for processes like midcell localization of protein clusters in some prokaryotic cells [9,31], directed motion of partition complexes [33], equidistant placing of plasmids along nucleoids [56], and maybe even transcription regulation [57].

We thank Dominik Schumacher and Lotte Sørensen for helpful discussions. We acknowledge financial support by the German Research Foundation (DFG) through TRR 174 (Project ID No. 269423233) and SFB1032 (Project ID No. 201269156) and the Excellence Cluster ORIGINS under Germany's Excellence Strategy (EXC-2094-390783311). During his time at Sorbonne University, L. D. has received funding from the European Union's Horizon 2020 research and innovation programme under the Marie Skłodowska-Curie grant agreement No. 860949. A. G. was supported by a DFG fellowship through the Graduate School of Quantitative Biosciences Munich (QBM). During his time at the Massachusetts Institute of Technology, A. G. was supported by the National Science Foundation (NSF) through Grant No. 2044895. I. M. has received funding from the European Union's Framework Programme for Research and Innovation Horizon 2020 under the Marie Skłodowska-Curie Grant Agreement No. 754388 (LMUResearchFellows) and from LMUexcellent, funded by the Federal Ministry of Education and Research (BMBF) and the Free State of Bavaria under the Excellence Strategy of the German Federal Government and the Länder.

L. D. and A. G. contributed equally to this work.

*Present address: Sorbonne Université, CNRS, Institut de Biologie Paris-Seine (IBPS), Laboratoire Jean Perrin (LJP), F-75005 Paris, France.

†Corresponding author.
andriy@goychuk.me

‡Present address: Institute for Medical Engineering and Science, Massachusetts Institute of Technology, Cambridge, Massachusetts 02139, USA.

§Corresponding author.
frey@lmu.de

- [1] C. P. Brangwynne, C. R. Eckmann, D. S. Courson, A. Rybarska, C. Hoege, J. Gharakhani, F. Jülicher, and A. A. Hyman, *Science* **324**, 1729 (2009).
- [2] A. A. Hyman, C. A. Weber, and F. Jülicher, *Annu. Rev. Cell Dev. Biol.* **30**, 39 (2014).
- [3] S. F. Banani, H. O. Lee, A. A. Hyman, and M. K. Rosen, *Nat. Rev. Mol. Cell Biol.* **18**, 285 (2017).
- [4] A. S. Lyon, W. B. Peeples, and M. K. Rosen, *Nat. Rev. Mol. Cell Biol.* **22**, 215 (2021).
- [5] S. Alberti, A. Gladfelter, and T. Mittag, *Cell* **176**, 419 (2019).
- [6] Y. Shin and C. P. Brangwynne, *Science* **357**, eaaf4382 (2017).
- [7] J.-M. Choi, A. S. Holehouse, and R. V. Pappu, *Annu. Rev. Biophys.* **49**, 107 (2020).
- [8] A. Klosin, F. Oltsch, T. Harmon, A. Honigmann, F. Jülicher, A. A. Hyman, and C. Zechner, *Science* **367**, 464 (2020).
- [9] D. Schumacher, S. Bergeler, A. Harms, J. Vonck, S. Huneke-Vogt, E. Frey, and L. Sørensen, *Dev. Cell* **41**, 299 (2017).
- [10] W. Ostwald, *Z. Phys. Chem.* **34U**, 495 (1900).
- [11] I. M. Lifshitz and V. V. Slyozov, *J. Phys. Chem. Solids* **19**, 35 (1961).
- [12] C. Wagner, *Z. Elektrochem.* **65**, 581 (1961).
- [13] A. J. Bray, *Adv. Phys.* **43**, 357 (1994).
- [14] C. A. Weber, D. Zwicker, F. Jülicher, and C. F. Lee, *Rep. Prog. Phys.* **82**, 064601 (2019).
- [15] S. C. Glotzer, D. Stauffer, and N. Jan, *Phys. Rev. Lett.* **72**, 4109 (1994).
- [16] S. C. Glotzer, E. A. Di Marzio, and M. Muthukumar, *Phys. Rev. Lett.* **74**, 2034 (1995).
- [17] J. J. Christensen, K. Elder, and H. C. Fogedby, *Phys. Rev. E* **54**, R2212 (1996).
- [18] D. Carati and R. Lefever, *Phys. Rev. E* **56**, 3127 (1997).
- [19] D. Zwicker, A. A. Hyman, and F. Jülicher, *Phys. Rev. E* **92**, 012317 (2015).
- [20] A. Lamorgese and R. Mauri, *Phys. Rev. E* **94**, 022605 (2016).
- [21] D. Zwicker, R. Seyboldt, C. A. Weber, A. A. Hyman, and F. Jülicher, *Nat. Phys.* **13**, 408 (2017).
- [22] J. D. Wurtz and C. F. Lee, *Phys. Rev. Lett.* **120**, 078102 (2018).
- [23] Y. I. Li and M. E. Cates, *J. Stat. Mech.* (2020) 053206.
- [24] J. Kirschbaum and D. Zwicker, *J. R. Soc. Interface* **18**, 20210255 (2021).
- [25] See Supplemental Material at <http://link.aps.org/supplemental/10.1103/PhysRevLett.130.128401> for further details and an additional analysis of the model, which includes Refs. [26–30].
- [26] A. Logg, K.-A. Mardal, G. N. Wells *et al.*, *Automated Solution of Differential Equations by the Finite Element*

- Method*, edited by A. Logg, K.-A. Mardal, and G. N. Wells (Springer, Berlin, Heidelberg, 2012).
- [27] M. Newville, T. Stensitzki, D. B. Allen, and A. Ingargiola, LMFIT: Non-linear least-square minimization and curve-fitting for Python (2014), [10.5281/zenodo.11813](https://doi.org/10.5281/zenodo.11813).
- [28] A. Meurer *et al.*, *PeerJ Comput. Sci.* **3**, e103 (2017).
- [29] Wolfram Research, Inc., *Mathematica*, Version 12.2, Champaign, IL, 2020.
- [30] L. Demarchi, A. Goychuk, I. Maryshev, and E. Frey, Source code—Enzyme-enriched condensates show self-propulsion, positioning, and coexistence (2023), [10.5281/zenodo.7347561](https://doi.org/10.5281/zenodo.7347561).
- [31] S. Bergeler and E. Frey, *PLoS Comput. Biol.* **14**, e1006358 (2018).
- [32] M. Kober, S. Bergeler, and E. Frey, *Biophys. J.* **117**, 420 (2019).
- [33] C. Hanauer, S. Bergeler, E. Frey, and C. P. Broedersz, *Phys. Rev. Lett.* **127**, 138101 (2021).
- [34] J.-F. Joanny and S. Ramaswamy, *J. Fluid Mech.* **705**, 46 (2012).
- [35] D. Khoromskaia and G. P. Alexander, *Phys. Rev. E* **92**, 062311 (2015).
- [36] C. A. Whitfield and R. J. Hawkins, *New J. Phys.* **18**, 123016 (2016).
- [37] R. Kree, P. S. Burada, and A. Zippelius, *J. Fluid Mech.* **821**, 595 (2017).
- [38] N. Yoshinaga, *J. Chem. Phys.* **150**, 184904 (2019).
- [39] S. Trinschek, F. Stegemerten, K. John, and U. Thiele, *Phys. Rev. E* **101**, 062802 (2020).
- [40] U. Thiele, K. John, and M. Bär, *Phys. Rev. Lett.* **93**, 027802 (2004).
- [41] K. John, M. Bär, and U. Thiele, *Eur. Phys. J. E* **18**, 183 (2005).
- [42] S. Michelin, *Annu. Rev. Fluid Mech.* **55**, 77 (2023).
- [43] J. W. Cahn, *Acta Metall.* **9**, 795 (1961).
- [44] S. R. De Groot and P. Mazur, *Non-Equilibrium Thermodynamics*, Dover Books on Physics (Dover Publications, New York, 2013).
- [45] R. Balian, *From Microphysics to Macrophysics* (Springer, Berlin, Heidelberg, 2007).
- [46] J. Halatek, F. Brauns, and E. Frey, *Phil. Trans. R. Soc. B* **373**, 20170107 (2018).
- [47] T. Burkart, M. C. Wigbers, L. Würthner, and E. Frey, *Nat. Rev. Phys.* **4**, 511 (2022).
- [48] D. Zwicker, *Curr. Opin. Colloid Interface Sci.* **61**, 101606 (2022).
- [49] M. E. Cates, in *Active Matter and Nonequilibrium Statistical Physics: Lecture Notes of the Les Houches Summer School* (Oxford Academic, Oxford, 2022), Vol. 112, [10.1093/oso/9780192858313.003.0006](https://doi.org/10.1093/oso/9780192858313.003.0006).
- [50] E. Frey and K. Kroy, *Ann. Phys. (Berlin)* **517**, 20 (2005).
- [51] A. Goychuk, L. Demarchi, I. Maryshev, and E. Frey, The role of non-reciprocity in the fluid-like dynamics of enzyme-enriched droplets (to be published).
- [52] R. A. Fisher, *Ann. Eugen.* **7**, 355 (1937).
- [53] F. Brauns, H. Weyer, J. Halatek, J. Yoon, and E. Frey, *Phys. Rev. Lett.* **126**, 104101 (2021).
- [54] H. Weyer, F. Brauns, and E. Frey, Coarsening and wavelength selection far from equilibrium: A unifying framework based on singular perturbation theory, [arXiv:2203.03892](https://arxiv.org/abs/2203.03892).
- [55] L. Rayleigh, *Proc. London Math. Soc.* **s1-10**, 4 (1878).
- [56] R. Ietswaart, F. Szardenings, K. Gerdes, and M. Howard, *PLoS Comput. Biol.* **10**, e1004009 (2014).
- [57] J. E. Henninger, O. Oksuz, K. Shrinivas, I. Sagi, G. LeRoy, M. M. Zheng, J. O. Andrews, A. V. Zamudio, C. Lazaris, N. M. Hannett, T. I. Lee, P. A. Sharp, I. I. Cissé, A. K. Chakraborty, and R. A. Young, *Cell* **184**, 207 (2021).